ELSEVIER

Journal of Photochemistry and Photobiology A: Chemistry 105 (1997) 135–148

Journal of PHOTOCHEMISTRY AND PHOTOBIOLOGY A:CHEMISTRY

Photoinduced intramolecular charge transfer in planar vs. twisted donor–acceptor terphenyls

S. Delmond [a], J.-F. Létard [a], R. Lapouyade [a,*], W. Rettig [b]

[a] *Laboratoire des Sciences Moléculaires, Institut de Chimie de la Matière Condensée de Bordeaux (ICMCB), UPR 9048 du CNRS, Château de Brivazac, Avenue du Dr. A. Schweitzer, 33608 Pessac Cedex, France*

[b] *Institute for Physical and Theoretical Chemistry, Humboldt University Berlin, Bunsenstrasse 1, D-10117 Berlin, Germany*

Received 15 July 1996; accepted 18 October 1996

Abstract

Photoinduced intramolecular charge transfer (ICT) was studied in 4-*N,N*-dibutylamino-4″-cyano-terphenyl and its conformationally more planar and more twisted analogues. Semi-empirical calculations (CNDO/S-CI) suggest that the twisted intramolecular charge transfer (TICT) states (A_2^* with the dimethylanilino group as the electron donor (D) perpendicular to the planar cyano diphenyl moiety (acceptor, A), A_3^* with the dimethylamino diphenyl group (D) perpendicular to the benzonitrile group (A) and $A_{2,3}^*$ with the three phenyl groups successively perpendicular such that D and A are parallel but linked by a phenyl group in a perpendicular relative conformation) are sufficiently low lying to become the lowest excited states in polar solvents because of their high dipole moments. Theoretical considerations suggest radiative properties for the TICT states A_2^* and A_3^* because of the large orbital coefficient at the single bond link and the possibility of strong coupling by deviation from perpendicularity. In contrast, non-radiative properties are suggested for the TICT state $A_{2,3}^*$ because D and A are separated by a neutral phenyl ring. The excited state dipole moments were obtained from the solvatochromic behaviour of the fluorescence. The decrease in the fluorescence quantum yields and the shortening of the fluorescence lifetimes in polar solvents (observed only for the sterically hindered compound) were analysed. The effect of a preferred non-planar ground state conformation has been accounted for by a different TICT state population and/or a modification of the TICT state emissive properties. © 1997 Elsevier Science S.A.

Keywords: Polar terphenyls; Radiative and non-radiative TICT states; Terphenyls

1. Introduction

During the last two decades, ample experimental evidence has been accumulated showing that photoinduced intramolecular charge transfer (ICT) plays a key role in the photophysics of donor–acceptor (D–A) substituted molecules. Indeed, on photoexcitation, conjugated organic molecules D–π–A, where an electron-donating group and an electron-withdrawing group interact through a π-conjugated system, can undergo a large change between the ground and excited state dipole moments ($\Delta\mu_{eg}$) due to a shift in the electron density from the D to the A group. Such a phenomenon has been reported in a number of D–A conjugated molecules, such as compounds derived from benzene [1–3], stilbenes [4–6], polyenes [7] and oligothiophenes [8].

Lengthening of the π-conjugated system connecting the D and A moieties is expected to increase the $\Delta\mu_{eg}$ term. In this context, push–pull polyenes behave as efficient electron transmitters, and it has been shown that the transition dipole moment $\Delta\mu_{eg}$ increases further with more than eight conjugated double bonds [7]. Nevertheless, polyene compounds are very unstable to light, and for application in the field of non-linear optics polyphenyls seem to be more appropriate with regard to stability. The non-planar equilibrium conformation, due to the balance between the conjugation of the aromatic groups and the steric repulsion between the hydrogen atoms of the bay region, is responsible for the significant blue shift of the absorption spectra of D–A polyphenyls ($D \equiv NMe_2$, $A \equiv NO_2$) when the number of phenyl groups is larger than two [9]. The first-order hyperpolarizability (β) increases with D–A *p*-terphenyls, and as a whole these compounds display an interesting compromise in terms of the non-linearity/transparency trade-off [9].

In the D–π–A series, one of the well-known compounds with one phenyl as the π spacer is 4-*N,N*-dimethylaminobenzonitrile (DMABN, $D \equiv NMe_2$ and $A \equiv CN$) [1–3], which

* Corresponding author.

PII S1010-6030(96)04544-3

leads to dual fluorescence in polar solvents, assigned to the presence of two emitting minima in the potential energy surface of the first excited state: the planar conformer, which is moderately polar and is called the ICT state in this study, and the perpendicular conformer (twisted intramolecular charge transfer (TICT) state [10]), characterized by full intramolecular electron transfer with π-orbital decoupling between the D (NMe_2) and A (benzonitrile) groups. However, Klock and Rettig [11] and Lahmani et al. [12,13] have shown that, at variance with DMABN, for the more elongated compound 4-*N*,*N*-dimethylamino-4′-cyano-biphenyl, only the nearly planar ICT state is formed, even in polar solvents.

In this paper, we investigate the ground state conformational effect associated with twisting around the two single bonds which link the D (*p*-*N*,*N*-dialkylanilino or *p*-*N*,*N*-dialkylaminobiphenyl) and A (*p*-cyanodiphenyl or *p*-benzonitrile) groups on the charge transfer character of 4-*N*,*N*-dialkylamino-4″-cyano-terphenyl in the excited state. The ICT excited state should not be much more stable than that of the biphenyl series, whereas a possible TICT state should have a larger dipole moment because of the increased distance between the separate charges and, in polar solvents, could become the lowest excited state.

In order to investigate the potential energy surface of the excited state and, in particular, to show the role of the putative TICT states, we synthesized the 4-*N*,*N*-dibutylamino-4″-cyano-terphenyl (DCT), where all the single bonds (1, 2 and 3, see Scheme 1) are free to rotate. The photophysical behaviour of this molecule was compared with that of the electronic equivalents, i.e. DCT-B2, where the single bond 2 is rigidized in the planar conformation by a methylene bridge, and DM-DCT, where two methyl groups bring about an increased φ_2 angle (for notation, see Scheme 1) because of the steric interactions between the CH_3 substituents and the hydrogen atoms in the bay position. In this paper, we focus on the solvent dependence of the spectral position of the fluorescence maximum (ν_{max}), the quantum yield (ϕ_f), the excited state depopulation kinetics (τ_f) and the resulting radiative (k_f) and non-radiative (k_{nr}) rate constants.

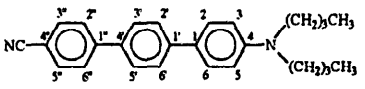

DCT

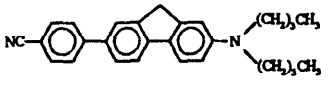

DCT-B2

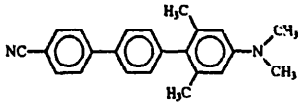

DM-DCT

A complementary technique for investigating the possible relaxation pathways on the potential energy surface of the first excited state involves quantum chemical calculations, which are used to obtain an idea of the excited state energies and dipole moments of the planar and various twisted conformers.

2. Experimental details

2.1. Apparatus and procedure

The absorption and emission spectra were recorded on Hitachi U-3300 and F-4500 spectrometers respectively. The standard for fluorescence quantum yield measurements was quinine bisulphate in 1 N H_2SO_4 ($\phi_f = 0.55$) and, after solvent refractive index correction, the experimental errors were estimated to be $\pm 10\%$. The fluorescence lifetimes were determined using synchrotron radiation from BESSY in the single bunch mode, described in detail elsewhere [14]. The statistical error for the lifetime measurements was smaller than 0.1 ns.

The solvents were of the highest quality commercially available from Merck or SDS. No fluorescence contaminants were detected on excitation in the wavelength region of

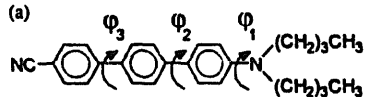

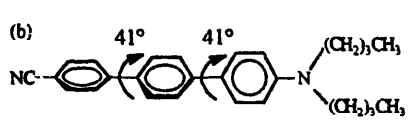

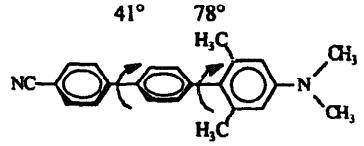

DCT **DM-DCT**

Scheme 1. (a) Molecular representation of DCT. The dihedral angles are denoted φ_i (φ_1, φ_2 and φ_3 with $0° \leq \varphi_i \leq 90°$) where the index *i* indicates the twisted bond. (b) Partially optimized φ_2 and φ_3 angles for DCT and DM-DCT in the ground state obtained by the AM1 method.

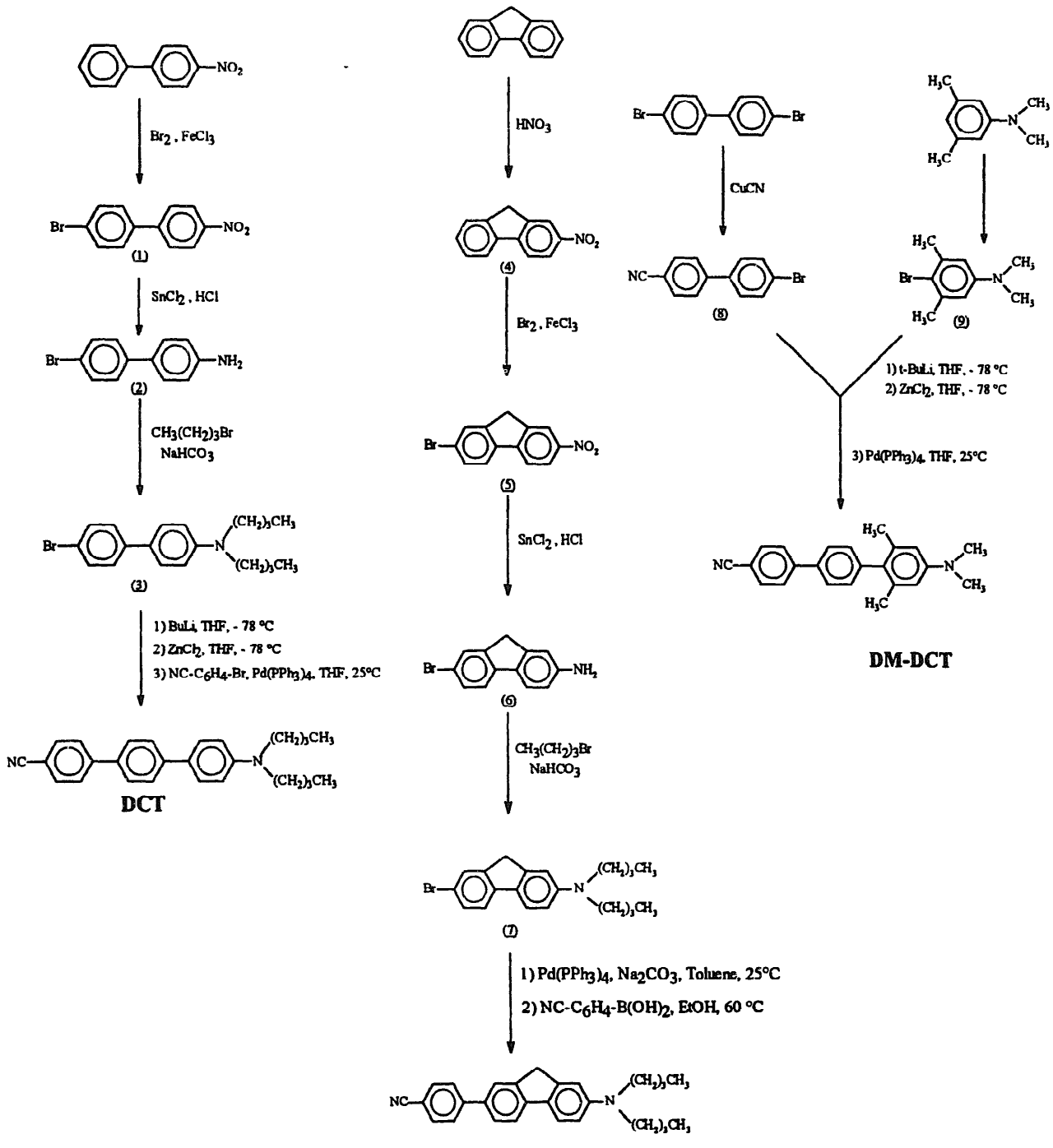

Fig. 1. Synthetic routes to 4-*N*,*N*-dibutylamino-4″-cyano-terphenyl (DCT), 2-*N*,*N*-dibutylamino-7-(*p*-benzonitrile)-fluorene (DCT-B2) and 2,6-dimethyl-4-*N*,*N*-dimethylamino-4″-cyano-terphenyl (DM-DCT).

experimental interest. The purity of the products was monitored by thin layer chromatography (TLC). Melting points (m.p.) were determined with a Mettler FR62 apparatus. ^{1}H Nuclear magnetic resonance (NMR) and ^{13}C NMR spectra were measured on a Bruker AC250 (250 MHz) instrument in $CDCl_3$ (Aldrich) solution.

2.2. Synthesis

4-*N*,*N*-Dibutylamino-4″-cyano-terphenyl (DCT), 2-*N*,*N*-dibutylamino-7-(4′-benzonitrile)-fluorene (DCT-B2) and 2,6-dimethyl-4-*N*,*N*-dimethylamino-4″-cyano-terphenyl (DM-DCT) are new compounds synthesized by the route outlined in Fig. 1. The last step is an aromatic–aromatic coupling, catalysed by Pd^0. For DCT and DM-DCT, the procedure described by Amatore et al. [15] from an organozinc and a bromo derivative was followed, whereas for DCT-B2, a borate precursor [16] was used because the fluorene derivative should deprotonate in basic solution.

Bromination of 4-nitro-biphenyl leads to 4-bromo-4′-nitro-biphenyl (1) [17]. 4-Amino-4′-bromo-biphenyl (2)

was prepared according to the procedure given by Blakey and Scarborough [18]. 4-*N,N*-Dibutylamino-4'-bromo-biphenyl (**3**) and 2-*N,N*-dibutylamino-7-bromo-fluorene (**7**) were obtained by alkylation of the amino derivatives by *n*-butyl-bromide. 2-Nitro-fluorene (**4**) [17] was prepared according to the method described by Kuhn [19]. 2-Nitro-7-bromo-fluorene (**5**) was obtained by following the procedure described by Case [17] for the preparation of 4-nitro-4'-bromo-biphenyl. 2-Nitro-7-bromo-fluorene was reduced to 2-amino-7-bromo-fluorene (**6**) with $SnCl_2$ in HCl, according to the synthesis described by Bellamy and Ou [20]. 4-Bromo-4'-cyano-biphenyl (**8**) [18] was prepared according to McNamara and Gleason [21]. 4-Bromo-3,5-dimethyl-*N,N*-dimethylaniline (**9**) was prepared by bromination of 3,5-dimethyl-*N,N*-dimethylaniline with 2,4,6,6-tetrabromo-2,5-cyclohexa-dien-1-one [22].

2.2.1. 4-N,N-Dibutylamino-4'-bromo-biphenyl (3)

In a three-necked flask containing *N,N*-dimethylformamide (DMF) (15 ml) was introduced successively, under argon, 4-amino-4'-bromo-biphenyl (**2**) (7.4 g, 30 mmol), butylbromide (16.4 g, 90 mmol) and $NaHCO_3$ (7.5 g, 90 mmol). The resulting mixture was heated overnight at 80 °C. The cooled solution was poured into iced water. The aqueous layer was extracted with Et_2O and the combined organic layers were washed to neutrality with water and dried over Na_2SO_4. The crude product was purified by chromatography on silica gel (petroleum ether–CH_2Cl_2, 7v/3v) to give a grey solid (4.2 g, 11.7 mmol, yield = 39%, m.p. = 84 °C). ^{1}H NMR ($CDCl_3$) δ (ppm): 1.15 (CH_3, t, 6H), 1.53 (CH_2, m, 4H), 1.76 (CH_2, m, 4H), 3.46 (CH_2, t, 4H), 6.86 (CH, d, 2H), 7.58 (CH, d, 2H), 7.59 (CH, m, 4H). ^{13}C NMR ($CDCl_3$) δ (ppm): 14.3 (CH_3), 20.6, 29.7, 51.0 (CH_2), 112.1, 127.8, 131.9 (CH), 119.8, 126.5, 140.4, 148.8 (C_q).

2.2.2. 4-N,N-Dibutylamino-4''-cyano-terphenyl (DCT)

In a three-necked flask, a solution of **3** (2.4 g, 7 mmol) in 10 ml of tetrahydrofuran (THF) was introduced under argon. At −78 °C, through a septum, a 2.5 M solution of BuLi (3.2 ml, 8 mmol) in *n*-hexane was added dropwise followed by a solution of $ZnCl_2$ (1 g, 7 mmol) in THF (10 ml). The resulting mixture was warmed to room temperature. $Pd(PPh_3)_4$ (460 mg, 0.4 mmol) and a solution of 4-cyano-bromobenzene (1 g, 6 mmol) in THF (5.6 ml) were introduced. After stirring overnight at room temperature, the mixture was poured onto water and extracted with CH_2Cl_2. The combined organic layers were washed with water and dried over Na_2SO_4. The crude product was purified by chromatography on silica gel (petroleum ether–CH_2Cl_2, 1v/3v) and recrystallized in a CH_2Cl_2–petroleum ether mixture to give a yellow powder (650 mg, 1.7 mmol, yield = 28%, m.p. = 210 °C). ^{1}H NMR ($CDCl_3$) δ (ppm): 1.01 (CH_3, t, 6H) 1.42 (CH_2, m, 4H), 1.64 (CH_2, m, 4H), 3.35 (CH_2, t, 4H), 6.76 (d, CH, 2H), 7.55 (d, CH, 2H), 7.65 (CH, m, 4H), 7.72 (CH, s, 4H). ^{13}C NMR ($CDCl_3$) δ (ppm): 14.1 (CH_3), 20.5, 29.5, 50.9 (CH_2), 111.9, 126.5, 127.4, 127.5, 127.8, 132.7 (CH), 110.5, 119.2, 126.4, 136.1, 141.7, 145.4, 148.0 (C_q).

2.2.3. 2-N,N-Dibutylamino-7-bromo-fluorene (7)

In a two-necked flask, 2-amino-7-bromo-fluorene (8 g, 41 mmol), 15 ml of DMF, butylbromide (16.8 g, 123 mmol) and $NaHCO_3$ (7.5 g, 92 mmol) were successively introduced under argon. The resulting mixture was heated overnight at 80 °C. The cooled solution was poured into iced water. The aqueous layer was extracted with Et_2O and the combined organic layers were washed to neutrality with water and dried over Na_2SO_4. The crude product was purified by chromatography on silica gel (petroleum ether–CH_2Cl_2, 7v/3v) to give a white solid (6 g, 16 mmol, 40%). ^{1}H NMR ($CDCl_3$) δ (ppm): 1.12 (CH_3, t, 6H), 1.52 (CH_2, m, 4H), 1.74 (CH_2, m, 4H), 3.43 (CH_2, t, 4H), 3.85 (CH_2, s, 2H), 6.79 (CH, d, 1H), 6.90 (CH, s, 1H), 7.49 (CH, s, 2H), 7.61 (CH, d, 1H), 7.64 (CH, s, 1H). ^{13}C NMR ($CDCl_3$) δ (ppm): 14.3 (CH_3), 20.6, 29.7, 37.1, 51.3 (CH_2), 108.2, 111.0 (CH), 117.9 (C_q), 119.5, 120.9, 127.9 (CH), 128.8 (C_q), 129.7 (CH), 141.8, 144.4, 145.1, 148.3 (C_q).

2.2.4. 2-N,N-Dibutylamino-7-(4'-benzonitrile)-fluorene (DCT-B2)

In a three-necked flask, a solution of 2-*N,N*-dibutylamino-7-bromo-fluorene (200 mg, 0.54 mmol) in 4.5 ml of toluene, $Pd(PPh_3)_4$ (38 mg, 0.033 mmol) and a 2 M aqueous solution of Na_2CO_3 (4.5 ml, 8.7 mmol) were successively introduced under argon. Through a septum, a solution of *p*-benzonitrile boric acid (110 mg, 0.75 mmol) in 2.1 ml of ethanol was added dropwise. The resulting mixture was heated under argon at 60–70 °C overnight and then extracted with Et_2O (3×30 ml). The combined organic layers were washed with brine and dried over sodium sulphate. The crude product was purified by flash chromatography (petroleum ether–CH_2Cl_2, 1/1) and recrystallized in a petroleum ether–CH_2Cl_2 (7/3) mixture to give a yellow–green powder (40 mg, 0.1 mmol, 20%). ^{1}H NMR ($CDCl_3$) δ (ppm): 1.00 (CH_3, t, 6H), 1.42 (CH_2, m, 4H), 1.64 (CH_2, m, 4H), 3.35 (CH_2, t, 4H), 3.90 (CH_2, s, 2H), 6.73 (CH, d, 1H), 6.86 (CH, s, 1H), 7.53 (CH, d, 1H), 7.61 (CH, s, 2H), 7.65 (CH, s, 1H), 7.72 (CH, s, 4H). ^{13}C NMR ($CDCl_3$) δ (ppm): 14.1 (CH_3), 20.4 (CH_2), 29.4 (CH_2), 37.2 (CH_2), 51.2 (CH_2), 108.1 (CH), 110.0 (C_q), 111.0 (CH), 118.6 (CH), 119.3 (C_q), 121.1 (CH), 126.0 (CH), 127.4 (CH), 132.5 (CH), 135.0 (C_q), 143.1 (C_q), 145.8 (C_q), 146.3 (C_q). MS (*m/z*): 394 (75%, $M^{\cdot+}$), 351 (100%), 309 (28%), 266 (21%), 155 (12%).

2.2.5. 2,6-Dimethyl-4-N,N-dimethylamino-4''-cyano-terphenyl (DM-DCT)

In a three-necked flask, a solution of 4-bromo-3,5-dimethyl-*N,N*-dimethylaniline (**5**) (1 g, 4 mmol) in THF (10 ml) was introduced under argon. At −78 °C, a 1.7 M solution of tert-BuLi in pentane (5.2 ml, 9 mmol) was added dropwise through a septum. After stirring at −78 °C for 30 min, a 1 M

solution of $ZnCl_2$ (4.4 ml, 4.4 mmol) in Et_2O was added. The resulting mixture was then warmed to room temperature and stirred for 1 h before adding successively a solution of 4-bromo-4'-cyano-biphenyl (930 mg, 4 mmol) in THF (10 ml) and a catalytic amount of $Pd(PPh_3)_4$ (280 mg, 0.2 mmol). The mixture was heated at 60–70 °C for 22 h and poured onto water. The aqueous layer was extracted with Et_2O and the combined organic layers were dried over Na_2SO_4. The crude product was purified by successive chromatographies on silica gel (petroleum ether–CH_2Cl_2, 7v/3v) to give a yellow solid (280 mg, 0.9 mmol, yield = 21%, m.p. = 190–200 °C). ^1H NMR ($CDCl_3$) δ (ppm): 2.09 (CH_3-C, s, 6H), 3.00 (CH_3-N, s, 6H), 6.57 (CH_{ar}, s, 2H), 7.29 (CH_{ar}, d, 2H), 7.66 (CH_{ar}, d, 2H), 7.76 (CH_{ar}, s, 4H). ^{13}C NMR ($CDCl_3$) δ (ppm): 21.5 (CH_3-C), 40.7 (CH_3-N), 111.8, 127.1, 127.6, 130.9, 132.7 (CH), 110.7, 119.1, 129.9, 136.8, 136.9, 142.2, 145.6, 149.8 (C_q). MS (m/z): 326 (100%, $M^{\cdot+}$).

2.3. Calculations

For the quantum chemical calculations, idealized bond lengths and angles were used, as defined previously [11,23]. The bond lengths of the single bonds 2 and 3 were taken to be equal to 1.485 Å and 1.494 Å respectively, as obtained by X-ray analysis of 4-*N*,*N*-diethylamino-terphenyl [24]. In DCT, the dibutylamino group was replaced by the electronically equivalent substituent NMe_2 in order to shorten the calculations.

The standard AM1 method within the AMPAC 5.0 package [25] was used to obtain the optimized geometry with respect to the dihedral angles (φ_1, φ_2 and φ_3, Scheme 1) and to calculate the energy (E_g, eV) and the dipole moment (μ_g, D) of the ground state. Several starting geometries were used for the geometry optimization to ensure that the optimized structure corresponds to a global minimum of φ_2 and φ_3 angles. Calculations were performed for different dihedral angles with all the other structural parameters kept constant at their values defined above. The energy of the optimized structure was used as a reference ($E_g = 0$ eV) for comparison with the ground state energies of other conformations. In view of the large angular energy changes obtained for the excited states, especially the solvated states (Section 3), the partial optimization of the comparatively flat ground state surface seems adequate.

Energy gaps between the ground and excited states (ΔE, eV) were calculated using the CNDO/S method [26], employing an updated version of QCPE program 333 as described previously [11]. The energies of the excited states were determined by adding these transition energies to the energy of the ground state at the corresponding conformation. For a short-hand notation, we call the conformers with the perpendicularly twisted single bond A_i (A_1, A_2, A_3 and $A_{2,3}$, with the index indicating the bond(s) twisted) and the lowest TICT excited states for these conformations A_i^* (A_1^*, A_2^*, A_3^* and $A_{2,3}^*$). All singly excited configurations lying below 15 eV (generally approximately 50) were taken into account in the CI procedure.

Since the primary purpose of this work was to determine whether the formation of a low-lying TICT state is possible for DCT and DM-DCT in polar media, the solvation energies of the excited states were calculated. The solvent was taken as a continuous dielectric continuum defined by the dielectric constant (ϵ). The energy of the solvated excited state E_e^s was estimated (Eq. (1)) according to Onsager theory [27,28]. In Eq. (1), E_g^{solv} and E_e^{solv} are the solvation energies of the ground and excited states respectively. The energy of the solvated ground state (E_g^s) is given by Eq. (2), and E_i^{solv} (i = g or e) is calculated according to Eq. (3), where μ_i denotes the dipole moment of the corresponding state i (calculated in the gas phase) [23,29]

$$E_e^s = E_g + \Delta E - E_e^{solv} + E_g^{solv} \quad (1)$$

$$E_g^s = E_g - E_g^{solv} \quad (2)$$

$$E_i^{solv} = \frac{\mu_i^2}{4\pi\epsilon_0\rho^3} f(\epsilon) \quad (3a)$$

with

$$f(\epsilon) = (\epsilon - 1)/(2\epsilon + 1) \quad (3b)$$

The Onsager cavity parameter ρ is determined for each compound from the molecular volume [6], calculated from the molecular weight and the density, which is assumed to be equal to unity (i.e. close to that of *N*,*N*-dimethylaniline (0.95 g cm^{-3}) [30] and benzonitrile (1.01 g cm^{-3}) [30]). This parameter, which represents the effective radius of the solvent shell around the molecule for the three compounds, has the following values: 5.3 Å (DCT), 5.4 Å (DCT-B2) and 5.1 Å (DM-DCT).

3. Results

3.1. Quantum chemical calculations

The results of the ground and excited state calculations for the planar and three perpendicular (A_1, A_2 and A_3) conformations for DCT and DM-DCT are summarized in Table 1.

For DCT, in the S_1 state, the planar conformation is the lowest. This state corresponds to the promotion of an electron from the highest occupied molecular orbital (HOMO) Ψ_{+1} (B symmetry) to the lowest unoccupied molecular orbital (LUMO) Ψ_{-1} (B symmetry), i.e. the transition denoted χ_1^{-1} belongs to the A symmetry within the C_2 operator (Fig. 2). The first TICT state, distinguished by a high dipole moment and a low oscillator strength, according to the principle of minimum overlap [31], is found to be an S_5 state at a considerably higher energy ($E_{S_5}^{A_3^*} = 5.3$ eV) than the planar S_1 state ($E_e = 4.2$ eV). The two TICT states (A_2^* and A_3^*) are very close in energy and in dipole moment, whereas A_1^* is clearly higher in energy (6.1 eV) and occurs as an S_7 state.

Table 1
Energies (E_g, eV) and dipole moments (μ_g, D) of the ground state (S_0) determined by AMPAC 5.0 calculations [25] for different conformations of DCT and DM-DCT. Energies (E_e, eV), oscillator strengths (f) and dipole moments (μ_e, D) of the excited states calculated by the CNDO/S method [26]. The symmetry (Sym.) within C_2 and the main configuration (χ_x^y) for each state are also listed

State	Parameter	Planar	Twisted A_1	Twisted A_2	Twisted A_3	Twisted $A_{2,3}$
DCT						
S_0^a	E_g	0.24	0.50	0.16	0.15	0.08
	μ_g	6.5	4.7	6.1	6.3	6.1
S_1	E_e	4.17	4.50	4.51	4.48	4.50
	μ_e	23.8	18.5	13.0	10.2	11.4
	f	0.8	0.8	0.71	0.004	0.02
	Sym. (χ_x^y)	A (χ_{+1}^{-1})	A (χ_{+1}^{-1})	A (χ_{+2}^{-1})	B (χ_{+1}^{-5})	B (χ_{+1}^{-5})
S_2	E_e	4.55	4.81	4.59	4.54	4.67
	μ_e	14.6	11.4	12.9	9.9	6.8
	f	0.0002	0.0009	0.002	0.02	0.12
	Sym. (χ_x^y)	B (χ_{+1}^{-4})	B (χ_{+1}^{-4})	B (χ_{+4}^{-1})	B (χ_{+1}^{-4})	B (χ_{+2}^{-3})
S_n^d	E_e		6.06 (S_7)[c]	5.33 (S_5)[c]	5.27 (S_5)[c]	6.26 (S_{13})[c]
	μ_e		41.0	44.5	43.9	51.8
	f		0	0	0	0.001
	Sym. (χ_x^y)		A (χ_{+5}^{-2})	A (χ_{+1}^{-1})	A (χ_{+1}^{-1})	A (χ_{+1}^{-1})
State	Parameter	Planar[e]	Twisted A_1^e	Twisted A_2	Twisted A_3^e	Twisted $A_{2,3}$
DM-DCT						
S_0^b	E_g	3.25	3.50	0.15	3.15	0.05
	μ_g	6.8	5.1	5.9	6.6	5.8
S_1	E_e	7.24	7.54	4.48	7.40	4.41
	μ_e	24.5	20.2	13.3	7.2	7.4
	f	0.79	0.79	0.71	0.009	0.01
	Sym. (χ_x^y)	A (χ_{+1}^{-1})	A (χ_{+1}^{-1})	A (χ_{+2}^{-1})	B (χ_{+1}^{-4})	B (χ_{+1}^{-4})
S_2	E_e	7.51	7.85	4.50	7.60	4.60
	μ_e	5.4	6.0	7.9	12.0	7.6
	f	0.004	0.0002	0.01	0.0008	0.02
	Sym. (χ_x^y)	B (χ_{+1}^{-4})	B (χ_{+1}^{-4})	B (χ_{+1}^{-4})	B (χ_{+1}^{-5})	B (χ_{+2}^{-3})
S_n^d	E_e		10.12 (S_{22})[c]	5.06 (S_5)[c]	8.21 (S_5)[c]	6.10 (S_{11})[c]
	μ_e		43.2	43.3	43.5	50.4
	f		0	0	0	0.00007
	Sym. (χ_x^y)		A (χ_{+1}^{-7})	A (χ_{+1}^{-1})	A (χ_{+1}^{-1})	A (χ_{+1}^{-1})

[a,b]The global minimum of the ground state (see Scheme 1), used as reference ($E_g = 0$ eV), is localized at $\varphi_2/\varphi_3 = 41°/41°$ for DCT[a] and $\varphi_2/\varphi_3 = 41°/78°$ for DM-DCT[b].
[c]Lowest lying TICT state for each conformation.
[d]First TICT state obtained.
[e]Calculated with $\varphi_2 = 0°$, yields an estimate of the steric destabilization for this planar geometry by the two *ortho*-methyl groups.

It is interesting to note that, for both TICT states A_2^* and A_3^*, the symmetry (A) and the main contribution (χ_1^{-1}) of the states are the same as for the strongly allowed S_1 state of the planar geometry (Fig. 2 and Table 1).

Whereas in the ground and first excited state (S_1) of DCT all the conformations (planar and perpendicular A_1–A_3 and $A_{2,3}^*$) are rather close in energy, for DM-DCT the perpendicular conformations A_2 and $A_{2,3}^*$ are clearly the lowest in energy, as expected from the steric interactions between the CH_3 substituents and the hydrogens in the bay position. The first low-lying TICT state, A_2^*, is found to be an S_5 state ($E_e = 5.1$ eV). The other TICT states (A_1^*, A_3^* and $A_{2,3}^*$) are higher in energy ($E_{S_5}^{A_3^*} = 8.2$ eV, $E_{S_{22}}^{A_1^*} = 10.1$ eV and $E_{S_{13}}^{A_{2,3}^*} = 6.3$ eV). As for DCT, the strongly allowed S_1 state of the planar conformation and the TICT state A_2^* of DM-DCT possess similar symmetry (A) and a χ_1^{-1} configuration as the main contribution.

The gas phase energies of the ground and excited states of DCT and DM-DCT, with the main χ_1^{-1} contribution, are presented in Fig. 3 as a function of the φ_2 and φ_3 angles. For the near-planar conformations, χ_1^{-1} corresponds to S_1. For the twisted conformations, it corresponds to the higher lying A_2^*, A_3^* and $A_{2,3}^*$ TICT states which, due to their large dipole moment, will be part of the S_1 surface in polar solutions. The other excited states have been calculated, but are not presented in Fig. 3 because of their very low dipole moments (see below); therefore they are not significantly stabilized when solvation is taken into account.

The ground state surface of DCT shows a wide distribution of conformers with a low energy difference (around 0.1 eV,

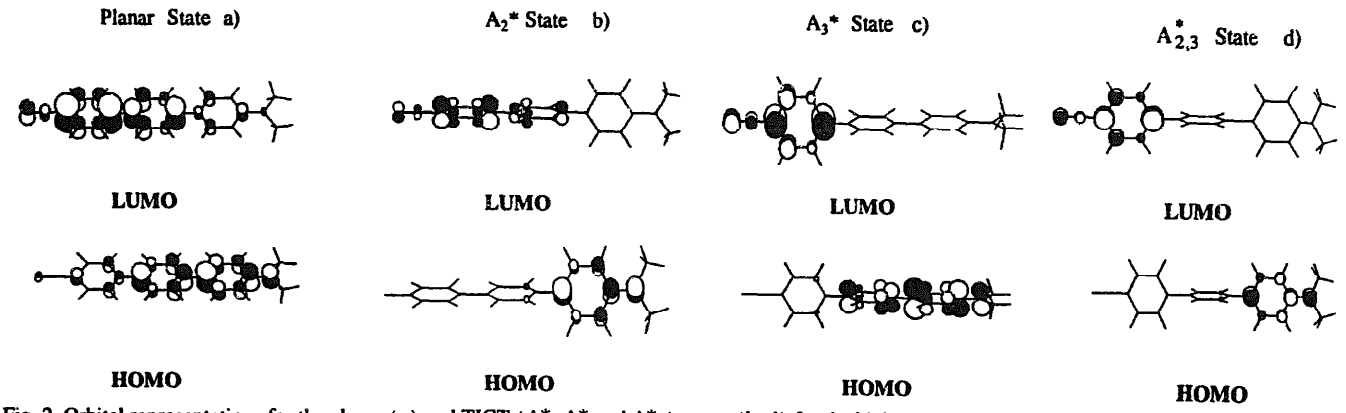

Fig. 2. Orbital representations for the planar (a) and TICT (A_2^*, A_3^* and $A_{2,3}^*$) states (b–d) for the highest occupied molecular orbital (HOMO) Ψ_{+1} and the lowest unoccupied molecular orbital (LUMO) Ψ_{-1} of DCT. (a) For the planar conformation, the configuration $\chi_+^-|$ (HOMO–LUMO transition) represents the preponderant weight of the S_1 state, with large oscillator strength and dipole moment ($f=0.79$ and $\mu_e=24.5$ D). (b) In the perpendicular TICT state A_2^*, the transition $\chi_+^-|$ (82% of weight involves a near one-electron transfer from the *p-N,N*-dimethylanilino to the cyano-biphenyl group) ($\Delta q=0.95$ of electronic charge), with large atomic orbital coefficients at bond 2 around which the donor and acceptor groups decouple, leads to a strong increase in the overlap integral on twisting away from the limiting 90° conformation. (c) The TICT state A_3^* ($\chi_+^-|$, 88%) involves an electron transfer from the 4-*N,N*-dimethylamino-biphenyl to the benzonitrile group ($\Delta q=0.97$), with strong sensitivity of the overlap integral to the twisting of bond 3. (d) The TICT state $A_{2,3}^*$ involves an electron transfer from the *p-N,N*-dimethylanilino to the benzonitrile group ($\Delta q=0.97$). It is important to note that, in contrast with A_2^* and A_3^*, the HOMO→LUMO overlap integral of the $A_{2,3}^*$ state is much less dependent on the twisting of bonds 2 and 3.

Fig. 3(a)), whereas DM-DCT (Fig. 3(b)) prefers a twisted conformation in the ground state with the dihedral angle φ_2 higher than 60° and φ_3 around 40°. In the ground state, the energy minima for DCT and DM-DCT occur around 40°/40° and 80°/40° (φ_2/φ_3) respectively (Fig. 3).

After initial excitation, both compounds relax to a more planar conformation. The minimum of the χ_1^{-1} hypersurface for DCT corresponds to φ_2/φ_3 of 20°/20° and for DM-DCT to 60°/20° (Table 2).

The contour map in Fig. 4 shows the evolution of the excited state dipole moment for the χ_1^{-1} hypersurface as a function of the angles φ_2 and φ_3. The minimum in the excited state (more planar than the ground state) possesses a notable dipole moment (Table 2), as a result of a partial intramolecular charge transfer, as illustrated in the planar conformation of DCT in Fig. 2. We call this minimum in the excited state the ICT state because it has a more planar conformation than the ground state and a significant excited state dipole moment.

A crude estimation of the solvation energy has been calculated from the dipole moment of the ground or excited state conformer and has been added to the excited state energy in the gas phase, yielding estimates for the changed sequence of excited states after solvation. However, solvent-induced changes in the wavefunction could not be taken into account for this level of approximation.

The χ_1^{-1} state of DCT in diethylether presents a flat surface for a φ_2 and/or φ_3 angle between 0° and 60° (Fig. 5(a)), with a slight minimum (attributed to the ICT state) at 30°. For DM-DCT, in contrast, the ICT state corresponds to a wide energy range around 60° for φ_2 and 40° for φ_3 (Fig. 5(b)), without being a real minimum, quite different to the gas phase (Fig. 3(b)). However, for both compounds, this surface presents some additional minima with regard to the gas phase for the perpendicular conformations A_2 and A_3 of DCT and A_2 of DM-DCT. Such results suggest that the corresponding TICT states may be involved in the photophysical properties of these dyes. In addition, for both compounds, a new TICT state $A_{2,3}^*$, in which the phenyl rings are successively in an orthogonal relation along the single bonds 2 and 3, appears as a minimum. This new TICT state ($A_{2,3}^*$) corresponds to a charge transfer from the *N,N*-dimethylaniline to the benzonitrile group (Fig. 2). It possesses an extremely large dipole moment (51.7 D for DCT and 50.4 D for DM-DCT) and presents the same symmetry (A) as the ICT, A_2^* and A_3^* states, but with small orbital coefficients over all the carbon atoms of the central phenyl ring (Fig. 2).

Thus, in diethylether, the semi-empirical calculations lead to several minima in the first excited state for both compounds: a charge transfer state (ICT state, moderately polar, more planar than the ground state) and several TICT states (A_2^*, A_3^* and $A_{2,3}^*$, highly polar).

The relative energies (ΔE_{ICT}^{TICT}) of the ICT and TICT (A_2^*, A_3^* and $A_{2,3}^*$) states for both compounds, as a function of the solvent polarity, are collected in Table 2. Although these values should be regarded as a qualitative guideline due to the uncertainty in the Onsager radius, the main features emerge clearly. In non-polar solvent (*n*-hexane), the ICT state is the lowest excited state for DCT ($\Delta E_{ICT}^{A_2^*}=+0.1$ eV, $\Delta E_{ICT}^{A_3^*}=+0.1$ eV), whereas for DM-DCT, the TICT (A_2^*) state becomes the lowest excited state ($\Delta E_{ICT}^{A_2}=-0.2$ eV). In polar solvents, such as acetonitrile, the TICT states A_2^*, A_3^* and $A_{2,3}^*$ are lower in energy than the ICT state. It should also be mentioned that solvation induces a clear change in the position of the ICT state towards a more twisted conformation in polar solvents, especially visible for DCT.

To summarize, the quantum chemical calculations lead to the following results relevant to fluorescence spectroscopy.

1. For DCT, in moderately polar and polar solvents, the TICT states A_2^* and A_3^* are lower in energy than the allowed ICT state. These two TICT states, which only differ in the

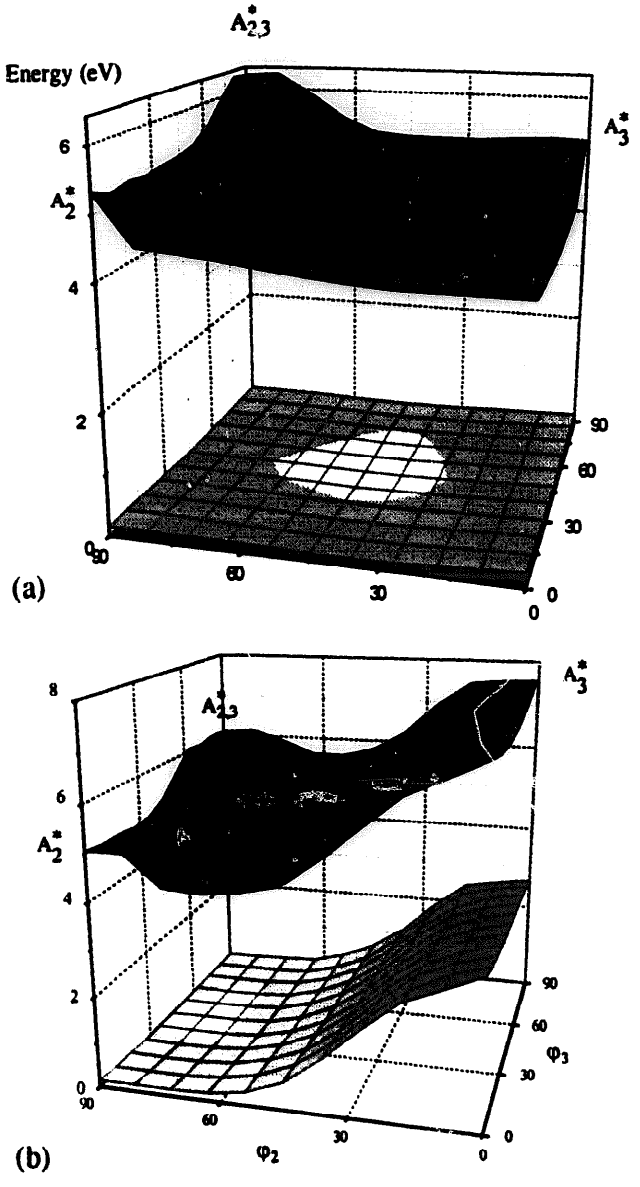

Fig. 3. Gas phase energies of the ground state (S_0) and of the first excited state with A symmetry and with χ_+^- as the main character for DCT (a) and DM-DCT (b) as a function of the internal rotation φ_2 and φ_3 from 0° to 90°. For all these calculations, the energies and dipole moments of the ground and excited states have been calculated every 20°, except when $\varphi_2 = 0°$ ($\varphi_3 = 0°$) where the calculations were made every 5° for $0° \leq \varphi_3 \leq 80°$ ($0° \leq \varphi_2 \leq 80°$) and every 2° for $80° \leq \varphi_3 \leq 90°$ ($80° \leq \varphi_2 \leq 90°$).

twisted bond, are very close in energy (see Fig. 5(a) and Table 2).

2. For DM-DCT, because of the steric interaction of the two CH_3 groups with the *ortho*-hydrogen atoms, there is an increase in the ICT state energy with respect to DCT. Thus, even in non-polar solvents, the TICT state A_2^* is lower in energy than the ICT state (Table 2). Therefore it can be predicted from the semi-empirical calculations that DM-DCT should populate a TICT state with a higher probability than DCT.
3. The TICT states A_1^* for both compounds and A_3^* for DM-DCT remain high in energy relative to the ICT or other TICT states, even in polar solvents, and are therefore probably not involved in the photophysics of these molecules.
4. The TICT state $A_{2,3}^*$ is sufficiently stabilized in polar solvents to become the lowest excited state for the two compounds. It should be noted that, for all the solvents, the energy difference between $A_{2,3}^*$ and the ICT state is larger for DM-DCT than for DCT. This corresponds to full charge transfer with very small orbital coefficients on all the carbons of the central phenyl ring, whereas the other TICT states A_2^* and A_3^* possess large orbital coefficients on the carbon atoms, which link the D (HOMO) and A (LUMO) groups (Fig. 2).

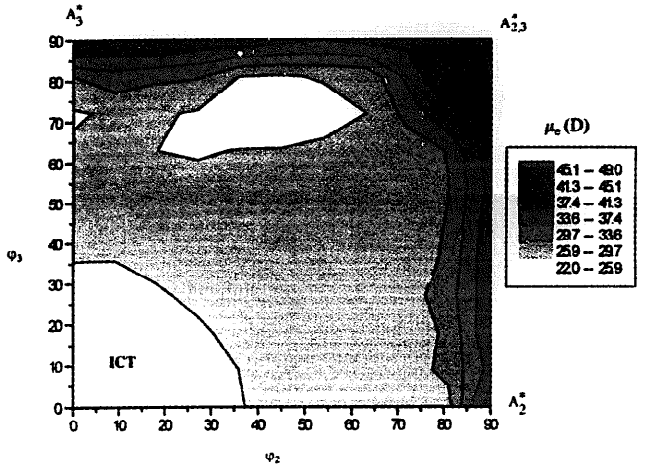

Fig. 4. Contour map of the excited state dipole moment for each conformation of DCT with angles φ_2 and φ_3. The relevant data of the planar and perpendicular conformations are listed in Table 2.

3.2. *UV–visible and fluorescence spectra*

The absorption maxima and fluorescence characteristics of DCT, DCT-B2 and DM-DCT are reported in Table 3.

The absorption spectra of the three compounds in acetonitrile are shown in Fig. 6. The absorption spectra of DCT and DCT-B2 are similar to that of 4-*N*,*N*-diethylamino-terphenyl ($\lambda_{max}^{abs}(CH_3CN) = 330$ nm [24]), with the expected red shift of the long-wavelength band due to stronger charge transfer character owing to the presence of the cyano group (DCT: $\lambda_{max}^{abs}(CH_3CH) = 360$ nm). Indeed, the lowest energy absorption band corresponds to a delocalized $\pi\pi^*$ excitation of high oscillator strength (DCT: $\epsilon(Et_2O) = 28\,130$ l mol^{-1} cm^{-1} and $\epsilon(CH_3CH) = 27\,540$ l mol^{-1} cm^{-1}). This conjugation band, polarized along the long axis, is blue shifted and has a small oscillator strength, appearing as a shoulder at 330 nm in DM-DCT ($\epsilon(CH_3CH) = 8100$ l mol^{-1} cm^{-1}), because of the large dihedral angle between the D and A moieties, which prevents the conjugation (Scheme 1 and Fig. 3(b)). On the other hand, the lowest energy absorption band is red shifted by about 15 nm (in acetonitrile) for DCT-B2 with respect to DCT because of the more planar conformation (in DCT-B2, $\varphi_2 = 0°$).

Table 2
Relative energies (eV) of the ground state (S_0) and the ICT and TICT (A_2^*, A_3^* and $A_{2,3}^*$) states and energy gaps (ΔE_{ICT}^{TICT}) in the gas phase and in solvents of various polarity for DCT and DM-DCT calculated using Eqs. (1)–(3). For the ground and ICT states, the corresponding angles φ_2/φ_3 for the energy minimum are shown and for all the states the dipole moments (D) are indicated

Compound	State	Parameter	Gas phase	*n*-Hexane	Et_2O	CH_3CN
DCT	S_0	φ_2/φ_3	41°/41°	41°/41°	41°/41°	41°/41°
		μ_g	6.3	6.3	6.3	6.3
	ICT[a]	φ_2/φ_3	20°/20°	20°/20°	40°/40°	60°/40°
		E_e	4.16	3.70	3.25	2.80
		μ_e	25.3	25.3	28.0	29.7
		f	0.78	0.78	0.75	0.72
	A_2^* (90°/0°)	E_e	5.33	3.82	2.52	1.43
		$\Delta E_{ICT}^{A_2^*}$	+1.17	+0.12	−0.73	−1.37
	A_3^* (0°/90°)	E_e	5.27	3.81	2.54	1.48
		$\Delta E_{ICT}^{A_3^*}$	+1.11	+0.11	−0.71	−1.32
	$A_{2,3}^*$ (90°/90°)	E_e	6.26	4.22	2.45	0.96
		$\Delta E_{ICT}^{A_{2,3}^*}$	+2.10	+0.52	−0.80	−1.84
DM-DCT	S_0	φ_2/φ_3	78°/41°	78°/41°	78°/41°	78°/41°
		μ_g	5.8	5.8	5.8	5.8
	ICT[a]	φ_2/φ_3	60°/20°	60°/20°	60°/40°[b]	60°/40°[b]
		E_e	4.34	3.68	3.06	2.52
		μ_e	28.1	28.1	29.6	29.6
		f	0.70	0.70	0.68	0.68
	A_2^* (90°/0°)	E_e	5.07	3.46	2.08	0.91
		$\Delta E_{ICT}^{A_2^*}$	+0.73	−0.22	−0.98	−1.61
	A_3^* (0°/90°)	E_e	8.21	6.78	5.54	4.50
		$\Delta E_{ICT}^{A_3^*}$	+3.87	+3.10	+2.48	+1.98
	$A_{2,3}^*$ (90°/90°)	E_e	6.11	3.93	2.05	0.46
		$\Delta E_{ICT}^{A_{2,3}^*}$	+1.77	+0.25	−1.01	−2.06

[a]The energy of the ICT state with A symmetry and χ_{-1}^{1} as main character is the lowest excited state.
[b]No real minimum with respect to transition towards the TICT state.

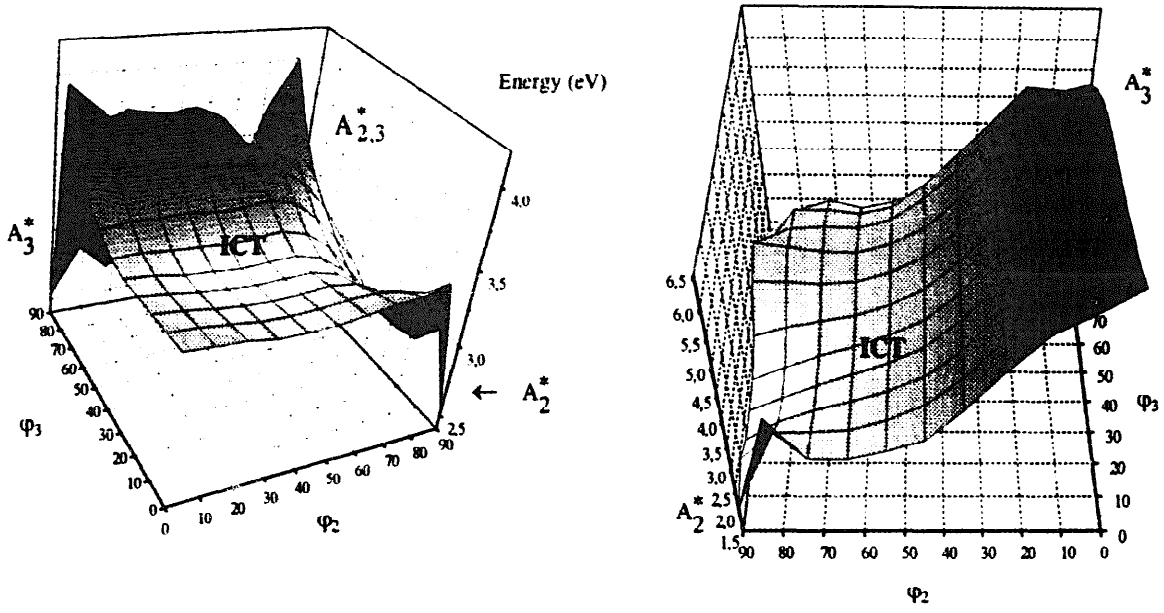

Fig. 5. Energies of the solvated excited S_1 state with A symmetry and χ_{+1}^{-1} character as a function of the dihedral angles φ_2 and φ_3 from 0° to 90° in diethylether for DCT (a) and DM-DCT (b). The solvation energies are calculated according to Eq. (3).

From non-polar to polar solvents we observe a small bathochromic shift of the absorption maxima (Table 3) and a large red shift of the fluorescence spectra of the three derivatives. In polar solvents, the fluorescence spectra are structureless and red shifted, whereas in non-polar solvents vibrational structure is observed, as illustrated in Fig. 7 for DCT.

The dipole moment of the emissive excited state can be estimated according to the treatment proposed in Refs. [32–34] (Eq. (4)), where $\Delta f' = [(\epsilon-1)/(2\epsilon+1)] -$

Table 3
Absorption (λ_{abs}^{max}, nm) and fluorescence (λ_{fluo}^{max}, nm) maxima, fluorescence quantum yields (ϕ_f) and fluorescence lifetimes (τ_f, ns) of DCT, DCT-B2 and DM-DCT in solvents of different polarity ($\Delta f' = (\epsilon-1)/(2\epsilon+1) - 0.5(n^2-1)/(2n^2+1)$) at room temperature. The radiative (k_f, $10^9\ s^{-1}$) and non-radiative (k_{nr}, $10^7\ s^{-1}$) rate constants determined using Eqs. (5) and (6) and the transition dipole moments (M, D) calculated using Eq. (7) are also listed

Compound	Solvent	$\Delta f'$	λ_{abs}^{max}	λ_{fluo}^{max}	ϕ_f^a	τ_f^b	k_f^c	k_{nr}^d	M^e
DCT	*n*-Hexane	0.09	352	406	0.79	1.2	0.66	17.6	7.2
	Et_2O	0.26	352	460	0.89	1.9	0.47	5.8	7.7
	THF	0.31	360	501	0.95	2.2	0.43	2.3	7.9
	CH_3CN	0.39	360	562	0.83	2.9	0.29	5.9	8.4
DCT-B2	*n*-Hexane	0.09	368	410	0.91	1.4	0.65	6.4	7.3
	Et_2O	0.26	371	454	0.78	2.0	0.39	11.0	7.0
	THF	0.31	377	505	0.70	2.1	0.33	14.0	7.0
	BuCN	0.37	378	546	0.71	2.6	0.27	11.0	7.3
	CH_3CN	0.39	375	565	0.78	2.8	0.28	7.9	8.1
DM-DCT	*n*-Hexane	0.09	267	408	0.48	1.4	0.34	36.8	5.2
	Et_2O	0.26	266	476	0.64	5.6	0.12	6.2	4.1
	THF	0.31	270	542	0.66	7.5	0.09	4.6	4.1
	BuCN	0.37	270	612	0.08	2.1	0.04	46	3.4
	CH_3CN	0.39	269	640	0.01	0.5	0.02	198	2.8

The experimental errors are ±10%[a], ±0.1 ns[b], $\pm 0.03\times10^9\ s^{-1}$ (Eq. (5))[c], $\pm 0.05\times10^7\ s^{-1}$ (Eq. (6))[d] and ±0.3 D (Eq. (7))[e].

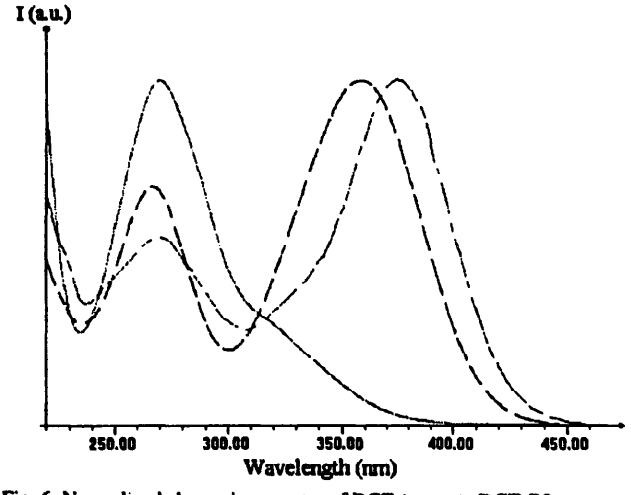

Fig. 6. Normalized absorption spectra of DCT (— —), DCT-B2 (— - — -) and DM-DCT (—) in acetonitrile. The molecular extinction coefficient (ϵ) of DCT at 358 nm is 27 540 l mol^{-1} cm^{-1} and that of DM-DCT at 267 nm is 34 670 l mol^{-1} cm^{-1}.

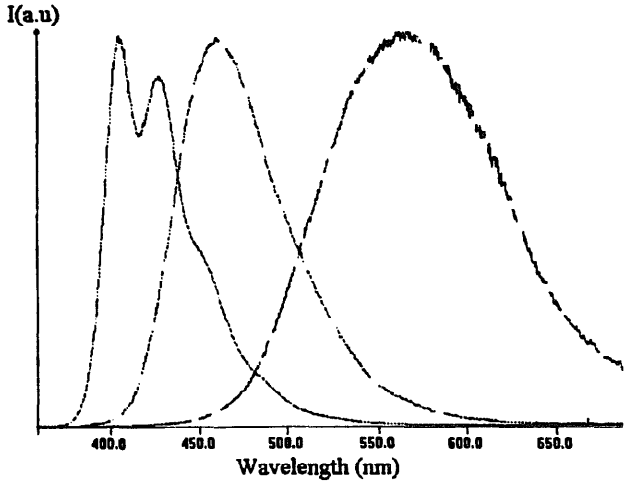

Fig. 7. Normalized fluorescence spectra of DCT as a function of the solvent polarity at room temperature in *n*-hexane (—), diethylether (— —) and acetonitrile (— - — -). The fluorescence quantum yields are listed in Table 3.

$0.5[(n^2-1)/(2n^2+1)]$ represents the solvent polarity parameter characterized by the dielectric constant ϵ and the optical refractive index n

$$\bar{\nu}_{fluo}^{max} = -2\mu_e(\mu_e-\mu_g)\frac{\Delta f'}{hc\rho^3} + \text{const}' \qquad (4)$$

The ground state dipole moment of all the molecules is taken to be equal to the value ($\mu_g = 6.2$ D) obtained by AM1 for the optimized geometry of DCT (see Section 2). The solvatochromic slope m of a plot of $\bar{\nu}_{fluo}^{max}$ vs. $\Delta f'$ yields the value of $2\mu_e(\mu_e-\mu_g)/hc\rho^3$ (Table 4). The magnitude of μ_e may be obtained from the slope by estimating the cavity radius (defined above) and the ground state dipole moment. The excited state dipole moments (μ_e) are collected in Table 4: they increase along the series DCT (21.7 D) < DCT-B2 (25.2 D) < DM-DCT (27.3 D). While the change in slope

Table 4
Solvatochromic slopes m (cm^{-1}), correlation coefficients (r), Onsager parameter ρ (Å), calculated from the mass density equation [35], and excited state dipole moments μ_e (D) for DCT, DCT-B2 and DM-DCT, derived from Eq. (4), taking into account the solvents listed in Table 3 with, in addition, dibutylether ($\Delta f' = 0.19$)

Compound	ρ	Slope m	r	μ_e^a
DCT	5.3[b]	23800	0.99	21.7
	4.9[c]	24880[c]	0.99[c]	22.8[c]
DCT-B2	5.4[b]	22670	0.99	25.2
DM-DCT	5.1	31830	0.99	27.3

[a] $\mu_g = 6.2$ D (see text).
[b] Calculation including the butyl groups.
[c] Values obtained with 4-*N*,*N*-dimethylamino-4″-cyano-terphenyl; they demonstrate the minor effect of the alkyl chain length.

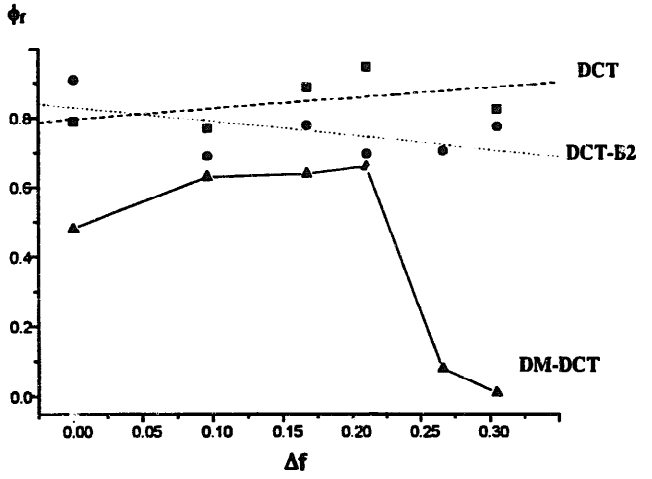

Fig. 8. Fluorescence quantum yields of DCT (■), DCT-B2 (●) and DM-DCT (▲) as a function of the solvent polarity ($\Delta f' = [(\epsilon-1)/(2\epsilon+1) - (n^2-1)/(2n^2+1)]$).

clearly indicates some difference between the three derivatives (Table 4), the absolute values of the excited state dipole moments should be viewed with caution, because of the uncertainty in the Onsager radius.

3.3. Fluorescence quantum yields and lifetimes and radiative and non-radiative rate constants

The fluorescence quantum yields (ϕ_f) of the terphenyl derivatives in various solvents are collected in Table 3 and Fig. 8. ϕ_f of DCT and DCT-B2 stays nearly constant at a high value whatever the solvent, whereas for DM-DCT ϕ_f decreases by a factor of 50 from *n*-hexane to acetonitrile. The decrease in the fluorescence quantum yield may result from a decrease in the rate constant of fluorescence (k_f) or an increase in the rate constant of radiationless deactivation (k_{nr}). The rate constant of fluorescence at room temperature is obtained experimentally as the ratio of the quantum yield of fluorescence to the lifetime (τ_f) according to Eq. (5), and the rate constant k_{nr} is derived from Eq. (6). In the latter equation, k_{nr} includes a possible pathway to the triplet state.

$$k_f = \frac{\phi_f}{\tau_f} \tag{5}$$

$$k_{nr} = k_f\left(\frac{1}{\phi_f} - 1\right) \tag{6}$$

The fluorescence lifetimes (τ_f) were measured at room temperature, near the fluorescence maximum, in various solvents (Table 3).

For the three compounds, a monoexponential decay is always observed at room temperature. The fluorescence lifetimes of DCT and DCT-B2 increase with the solvent polarity (for DCT, 1.2 ns in *n*-hexane to 2.9 ns in CH_3CN), whereas for DM-DCT, after an increase in τ_f from *n*-hexane (1.4 ns) to THF (7.5 ns), a strong decrease is observed in polar solvents (CH_3CN, $\tau_f = 0.5$ ns).

The radiative rate constant of fluorescence (k_f) (Eq. (5)) and k_{nr} data (Eq. (6)) obtained at room temperature are listed in Table 3. For the three compounds, k_f decreases as the solvent polarity increases, but more strongly for DM-DCT. The transition dipole moments *M*, which are related to the radiative rate constant by Eq. (7) [36], are reported in Table 3

$$k_f = \frac{64\pi^4}{3h} n^3 \bar{\nu}_f^3 |M|^2 \tag{7}$$

For DCT and DCT-B2, the transition dipole moments *M* increase significantly with increasing polarity of the solvent (outside the experimental error).

While there is no influence of the solvent polarity on the absorption coefficient for the shoulder at 330 nm of DM-DCT ($\log \epsilon$(*n*-hexane) = 4.49 l mol^{-1} cm^{-1} and $\log \epsilon(CH_3CN) = 4.54$ l mol^{-1} cm^{-1}), the transition dipole moment (*M*) of the fluorescent state strongly decreases in polar solvents, indicating a change in the electronic structure of the emitting state due to interaction with the polar solvent.

The non-radiative rate constants are nearly solvent independent for DCT and DCT-B2, but there is a strong increase in k_{nr} in more polar solvents than THF for DM-DCT. Except for DCT-B2, k_{nr} is also enhanced in the non-polar solvent *n*-hexane.

4. Discussion

With the help of the semi-empirical calculations, the results of solvatochromism, fluorescence quantum yields and lifetimes vs. solvent polarity at room temperature can be discussed within the two-state model first proposed by Rettig and Majenz [37] for the D–A stilbene series.

The absorption spectra of the terphenyls (DCT, DCT-B2 and DM-DCT) can be explained by the modification of the molecular geometry in the ground state due to the change in the torsional angles between the aromatic moieties. In these molecules, the ground state conformation is the result of a balance between two opposite effects: (1) conjugation between the aromatic rings which is at a maximum for the planar geometry; (2) repulsion between the proximate hydrogen atoms in the bay regions, which favours twisting around the inter-ring C–C bonds. As a consequence, terphenyl derivatives and, more generally, poly(*p*-phenylene) oligomers [38] are non-planar in the ground state. For DCT, we have calculated the equilibrium torsion angles φ_2 and φ_3 to be near 40°, while they have been measured to be $\varphi_2 = 29.9°$ and $\varphi_3 = 23.3°$ in 4-*N*,*N*-dimethylamino-terphenyl from crystal structure data [24]. Such a deviation between X-ray data and theoretical calculations, which has often been observed for the polyphenyl series, can be explained as a result of competition between two interactions: intramolecular repulsion between the *ortho*-hydrogen atoms on adjacent phenyl rings and intermolecular packing forces in the crystal, which

tend to restore planarity in order to optimize the packing between the molecules [39].

The absorption spectrum of DCT is similar to the absorption spectrum of the parent *p*-terphenyl [40], with the expected red shift from the D–A interaction; however, for DM-DCT, a blue shift is observed because of the steric interactions, which decouple the dimethylanilino group from the cyano-biphenyl part of the molecule.

In contrast, a strong red shift of the fluorescence spectrum occurs in polar solvents for the three compounds. This bathochromic shift is more pronounced for DM-DCT, as recently illustrated in the biphenyl series [41,42], and points to a larger excited state dipole moment associated with the quasi-orthogonal geometry of the D and A part in DM-DCT.

Semi-empirical calculations of the excited state energies in the gas phase for DCT and DM-DCT show that the lowest excited state corresponds to a nearly planar conformation. When the solvation energy is taken into account, the minimum of the ICT state in DCT shifts to higher angles (Table 2). This results from the increase in the excited dipole moment at intermediate φ_2/φ_3 angles compared with the planar conformation, as illustrated by the contour map of the excited state dipole moment presented in Fig. 4. For DM-DCT, the geometry of the ICT state is changed only at bond 3 with the solvent polarity; φ_2 keeps a value close to 60° (without a real minimum in polar solvents), whereas φ_3 shifts from 20° in the gas phase to 40° in acetonitrile (Table 2).

The calculations indicate that, for DCT, the TICT states A_2^*, A_3^* and $A_{2,3}^*$ are sufficiently stabilized in polar solvents to become photophysically relevant, whereas for DM-DCT, only A_2^* and $A_{2,3}^*$ can be photochemically active. Indeed, these calculations predict a population of these states for solvents more polar than diethylether for DCT and in *n*-hexane for DM-DCT (Table 2). However, experimentally, the fluorescence quantum yields and radiative transition moments *M* of DCT and DCT-B2 are nearly unaffected by the solvent polarity (Table 3), whereas for DM-DCT, a strong decrease occurs when the polarity of the solvent is equal to or higher than that of THF (Fig. 8). Let us first examine the case of DCT and DCT-B2.

The high fluorescence quantum yields of DCT and DCT-B2, observed in all the solvents investigated (Table 3 and Fig. 8), are due to the strongly allowed transition of the ICT state, as shown by the *M* values. Similar results have been described recently for 4-*N*,*N*-dimethylamino-4′-cyano-biphenyl [41,42]. Nevertheless, a clear increase in the *M* values is observed with increasing solvent polarity which indicates an increase in the allowed character for the emitting excited state(s). Taking into account the broad angular distributions, the effective k_f can be written as $k_f = \int_\theta f(\theta) n(\theta) d\theta$, i.e. the observable k_f value derives from a convolution of the angular distribution function $n(\theta)$ with the angle-dependent *f* value [43].

Theoretical calculations predict for DCT (and for DCT-B2) the population of TICT states A_2^*, A_3^* and $A_{2,3}^*$ in polar solvents, and a global decrease in the *M* values is expected. The opposite experimental result could indicate an overestimation of the solvent stabilization (due to an Onsager radius in Eq. (3) which is too small), and A_2^*, A_3^* and $A_{2,3}^*$ may not be sufficiently stabilized to become significantly populated.

However, global analysis of the time-resolved fluorescence of the biphenyl system DM-DCB [42] indicates the TICT state A_2^* as an emissive species with a reduced transition moment. Preliminary results on DCT and DCT-B2 in low-temperature polar solvents also indicate more than one emissive state [44]. The increase in the *M* values in polar solvents due to the change in the ICT geometry can mask the population of the TICT state, in particular if the TICT transition is strongly allowed. For small deviations from 90° (a realistic representation of a TICT rotational distribution [2,3,45]), the π orbitals on D and A start to overlap if large coefficients are present at the linking atoms, and we can expect for the A_2^* and A_3^* states large coefficients at this carbon (Fig. 2) allowing coupling with the ICT state from which they borrow their allowedness.

For DM-DCT, only the population of the TICT state A_2^* is relevant if we disregard $A_{2,3}^*$ for a moment. However, the decrease in the *M* values with the solvent polarity is different from the behaviour observed for DCT and DCT-B2. Various interpretations can be proposed.

1. The kinetic population of the TICT state from the ICT state is faster for DM-DCT than for DCT and DCT-B2. The semi-empirical calculations, when solvation is taken into account, suggest a higher energy difference between ICT and TICT for DM-DCT than for DCT (Table 2) and a correspondingly smaller activation energy. For DM-DCT, even in non-polar solvents, the TICT state is calculated to be the lowest. This preferred stabilization of the TICT state for DM-DCT, which has a similar excited state dipole moment (μ_{A2}^*(DCT) = 44.5 D and μ_{A2}^*(DM-DCT) = 43.3 D), results from the lower energy difference in the gas phase between the ICT and TICT states (Table 2).
2. The decrease in the radiative transition moment as a function of the solvent polarity has also been observed in other diaryls, i.e. for compounds which are confined to a non-planar geometry, such as 4-(*p*-*N*,*N*-dimethylanilino)-1-cyano-naphthalene [12,13], 2,6-dimethyl-4-*N*,*N*-dimethylamino-4′-cyano-biphenyl [41,42], 9-(*p*-*N*,*N*-dimethylanilino)-phenanthrene [43], 9-(*p*-*N*,*N*-dimethylanilino)-anthracene [46] and 4-[2′-pyrenyl]-benzaldehyde [47]. This effect has been interpreted by an increase in the proportion of a less allowed conformation, which is related to an angular relaxation process towards a more twisted geometry. However, in view of the solvent-independent calculated *f* values as a function of the rotational angle (Table 2), we conclude that the properties of the ICT state alone cannot explain the reduction in the *M* values observed for DM-DCT in more polar solvents.
3. Finally, in addition to the TICT states A_2^* and A_3^*, the calculations predict a further minimum (TICT state $A_{2,3}^*$)

in polar solvents, which may be photophysically relevant for DM-DCT. The orbital properties of $A^*_{2,3}$ (Fig. 2), with vanishing coefficients in the central ring, suggest that the vibronic coupling between ICT and TICT, allowed by the non-zero width of the rotational distribution function, will be weak or absent, and very low effective M values are expected.

5. Conclusions

Three new D–A terphenyl derivatives (DCT, DCT-B2 and DM-DCT) have been synthesized. The photophysical properties of these compounds have been measured in various solvents and discussed with the help of quantum chemical calculations.

The ground state conformational geometry has been calculated by the AM1 method and the energy minima (φ_2/φ_3) for DCT-B2, DCT and DM-DCT are 0°/41°, 41°/41° and 78°/41° respectively. The CNDO/S calculations indicate that emissive TICT (A^*_2 and/or A^*_3) states may be populated for the three derivatives, when solvation is taken into account. In addition, a non-emissive TICT state $A^*_{2,3}$ is also sufficiently low lying in polar solvents to become photophysically relevant.

The bathochromic shift of the emission spectra in polar solvents and the resulting dipole moment values provide clear evidence that the fluorescent excited state has a pronounced charge transfer character.

For DM-DCT, the transition moment M decreases strongly when the solvent polarity increases. This result has been attributed to a higher proportion of TICT population with respect to DCT, a less allowed character of the TICT state for DM-DCT (A^*_2) and/or the population of a doubly perpendicular TICT state $A^*_{2,3}$ with more forbidden character. The strong increase in the non-radiative rate constant (k_{nr}) in polar solvents, observed only for DM-DCT, points to the specific properties of the TICT state $A^*_{2,3}$ with regard to those of A^*_2 and/or A^*_3.

Acknowledgements

We wish to thank Michael Maus for many fruitful discussions. This work was supported by the BMFT project 05 414 SKT FAB9, the EC Large Scale Installations Programme (GE 1-0018-D(B)) and the Foreign Offices of Germany and France (Procope). We thank Professor Th. Bally (Fribourg) for the program MOPLOT.

References

[1] E. Lippert, W. Lüder, F. Moll, H. Nagele, H. Boos, H. Prigge and I. Siebold-Blankenstein, *Angew. Chem., 73* (1961) 695. E. Lippert, W. Lüder and H. Boos, in A. Mangini (ed.), *Advances in Molecular Spectroscopy, European Conference on Molecular Spectroscopy, Bologna, Italy, 1959*, Pergamon, Oxford, 1962, p. 443.
[2] W. Rettig, *Angew. Chem. Int. Ed. Engl., 25* (1986) 971.
[3] W. Rettig, in J. Mattay (ed.), *Topics in Current Chemistry, Vol. 169, Electron Transfer I*, Springer, Berlin, 1994, p. 253.
[4] R. Lapouyade, A. Kuhn, J.-F. Létard and W. Rettig, *Chem. Phys. Lett., 208* (1993) 48.
[5] R. Lapouyade, K. Czeschka, W. Majenz, W. Rettig, E. Gilabert and C. Rullière, *J. Phys. Chem., 96* (1992) 9643.
[6] J.-F. Létard, R. Lapouyade and W. Rettig, *J. Am. Chem. Soc., 115* (1993) 2441.
[7] A. Slama-Schwock, M. Blanchard-Desce and J.-M. Lehn, *J. Phys. Chem., 94* (1990) 3894.
[8] F. Würthner, F. Effenberger, R. Wortmann and P. Krämer, *Chem. Phys., 173* (1993) 305.
[9] I. Ledoux, J. Zyss, A. Jutand and C. Amatore, *Chem. Phys., 150* (1991) 117.
[10] K. Rotkiewicz, K.H. Grellmann and Z.R. Grabowski, *Chem. Phys. Lett., 19* (1973) 315; erratum: *Chem. Phys. Lett., 21* (1973) 212.
[11] A.M. Klock and W. Rettig, *Polish J. Chem., 67* (1993) 1375.
[12] F. Lahmani, E. Bréhéret, A. Zehnacker-Rentien, C. Amatore and A. Jutand, *J. Photochem. Photobiol. A: Chem., 70* (1993) 39.
[13] F. Lahmani, E. Bréhéret, O. Benoist d'Azy, A. Zehnacker-Rentien and J.F. Delouis, *J. Photochem. Photobiol. A: Chem., 89* (1995) 191.
[14] M. Vogel and W. Rettig, *Ber. Bunsenges. Phys. Chem., 91* (1987) 1241.
[15] C. Amatore, A. Jutand and S. Negri, *J. Organomet. Chem., 390* (1990) 389.
[16] N. Miyaura, T. Yanagi and A. Suzuki, *Synth. Commun., 11* (1981) 513.
[17] F.H. Case, *J. Am. Chem. Soc., 60* (1938) 424.
[18] W. Blakey and H.A. Scarborough, *J. Chem. Soc., II* (1927) 1401.
[19] W.E. Kuhn, *Org. Synth., 447* (1943).
[20] F.D. Bellamy and K. Ou, *Tetrahedron Lett., 25* (1984) 839.
[21] J.M. McNamara and W.B. Gleason, *J. Org. Chem., 41* (1976) 1071.
[22] G.J. Fox, J.D. Hepworth and G. Hallas, *J. Chem. Soc., Perkin Trans. I*, (1973) 68.
[23] J.-F. Létard, R. Lapouyade and W. Rettig, *Chem. Phys., 186* (1994) 119–131.
[24] M.J. Foley and L.A. Singer, *J. Phys. Chem., 98* (1994) 6430.
[25] AMPAC 5.0, ©1994 Semichem, 7128 Summit, Shawnee, KS 66216, USA.
[26] J. Del Bene and H.H. Jaffé, *J. Chem. Phys., 48* (1968) 1807, 4050; *49* (1968) 1221; *50* (1969) 1126.
[27] L. Onsager, *J. Am. Chem. Soc., 58* (1936) 1486.
[28] C.J.F. Böttcher, *Theory of Electric Polarization*, Vol. 1, Elsevier, Amsterdam, 2nd edn., 1973.
[29] D. Majumdar, R. Sen, K. Bhattacharyya and S.P. Bhattacharyya, *J. Phys. Chem., 95* (1991) 4324.
[30] D.R. Lide (ed.), *Handbook of Chemistry and Physics*, CRC Press, London, Tokyo, 75th edn., 1995.
[31] E. Lippert, W. Rettig, V. Bonacic-Koutecky, F. Heisel and J.A. Miehé, *Adv. Chem. Phys., 68* (1987) 1.
[32] W. Liptay, *Z. Naturforsch., 20* (1965) 1441.
[33] N. Mataga, Y. Kaifu and K. Koizumi, *Bull. Chem. Soc. Jpn., 29* (1956) 465.
[34] W. Baumaun, H. Bischof, J.-C. Fröhling, C. Brittinger, W. Rettig and K. Rotkiewicz, *J. Photochem. Photobiol. A: Chem., 64* (1992) 49.
[35] M.M. Karelson and M.C. Zerner, *J. Phys. Chem., 96* (1992) 6950. A. Broo and M.C. Zerner, *Chem. Phys. Lett., 227* (1994) 551. A. Broo and M.C. Zerner, *Theor. Chim. Acta, 90* (1995) 383.
[36] J.B. Birks, *Photophysics of Aromatic Molecules*, Wiley, New York, 1970, p. 48.
[37] W. Rettig and W. Majenz, *Chem. Phys. Lett., 154* (1989) 335.
[38] K.N. Backer, A.V. Fratini, T. Resch, H.C. Knachel, W.W. Adams, E.P. Socci and B.L. Farmer, *Polymer, 34* (1993) 1571.

[39] H. Cailleau, J.L. Baudour, J. Meinnel, A. Dworkin, F. Moussa and C.M.E. Zeyen, *Faraday Discuss. Chem. Soc., 69* (1980) 7.
[40] H. Jaffe and M. Orchin, *Theory and Applications of Ultraviolet Spectroscopy*, Wiley, New York, 1966.
[41] M. Maus, W. Rettig and R. Lapouyade, *J. Information Recording, 22* (1996) 451.
[42] M. Maus, W. Rettig, D. Bonafoux and R. Lapouyade, in preparation.
[43] A. Onkelinx, F.C. De Schryver, L. Viaene, M. Van der Auweraer, K. Iwai, M. Yamamoto, M. Ichikawa, H. Masuhara, H. Maus and W. Rettig, *J. Am. Chem. Soc., 118* (1996) 2892.
[44] S. Delmond, J.-F. Létard, R. Lapouyade and W. Rettig, in preparation. S. Delmond, J.-F. Létard and R. Lapouyade, *International Meeting of Physical Chemistry: Intra- and Inter-molecular Photoprocesses of Conjugated Molecules, Riccione, Italy, 14–18 July, 1996.*
[45] M. Van der Auweraer, Z.R. Grabowski and W. Rettig, *J. Phys. Chem., 95* (1991) 2083.
[46] J. Herbich and A. Kapturkiewicz, *Chem. Phys., 170* (1993) 221.
[47] J. Dobkowski, J. Waluk, W. Yang, C. Rullière and W. Rettig, *New J. Chem.*, submitted for publication.